

Review

Fabrication and SERS Performances of Metal/Si and Metal/ZnO Nanosensors: A Review

Grégory Barbillon 

EPF-Ecole d'Ingenieurs, 3 bis rue Lakanal, 92330 Sceaux, France; gregory.barbillon@epf.fr

Received: 5 January 2019; Accepted: 28 January 2019; Published: 30 January 2019



Abstract: Surface-enhanced Raman scattering (SERS) sensors are very powerful analytical tools for the highly sensitive detection of chemical and biological molecules. Substantial efforts have been devoted to the design of a great number of hybrid SERS substrates such as silicon or zinc oxide nanosystems coated with gold/silver nanoparticles. By comparison with the SERS sensors based on Au and Ag nanoparticles/nanostructures, higher enhancement factors and excellent reproducibilities are achieved with hybrid SERS nanosensors. This enhancement can be due to the appearance of hotspots located at the interface between the metal (Au/Ag) and the semiconducting substrates. Thus, in this last decade, great advances in the domain of hybrid SERS nanosensors have occurred. In this short review, the recent advances of these hybrid metal-coated semiconducting nanostructures as SERS sensors of chemical and biological molecules are presented.

Keywords: SERS; sensors; plasmonics; silicon; zinc oxide; metals

1. Introduction

Since the 2000s, surface enhanced Raman scattering (SERS) spectroscopy based on a nanostructured substrate has become a powerful and promising technique for highly sensitive detection of chemical/biological molecules [1–4]. SERS performance depends on the substrates, which are mainly realized with metallic nanoparticles [5–9] or nanostructures [10–12] with different geometries obtained by various techniques such as X-ray interference lithography [13], interference lithography [14,15], deep UV lithography [16,17] and electron beam lithography [18–20]. Large SERS enhancement ability and reproducibility are achieved by these techniques. However, they require costly equipment and heavy manufacturing processes for mass production. Several low-cost strategies such as nanosphere lithography [21–23], nanoimprint lithography [24–26] and metallic nanoparticle assemblies by self-assembling processes [27–29] are employed as an alternative method for industrial production. Nonetheless, a limiting factor of these two low-cost techniques is the definition of nanostructures on large surfaces. More recently, alternative and promising SERS substrates have emerged and are composed of silicon nanowires associated with metallic nanoparticles [30–40] showing ultrahigh sensitivity and excellent reproducibility. For example, Galopin et al. investigated silicon nanowires coated with silver nanoparticles on large surfaces [38]. In addition, another alternative solution is to choose zinc oxide (ZnO) nanostructures. Indeed, this semiconducting material can be applied to SERS sensing [41–44] because ZnO has an excellent propensity for nanostructuration combined with a relatively high refractive index, which better confines the light and thus induces a potential enhancement of the SERS effect as for the silicon having also a high refractive index. For instance, Sinha et al. investigated ZnO nanorods coated with a gold layer [42]. Compared with SERS substrates only based on pure Au or Ag nanoparticles which have relatively low values of enhancement factors (EF), both hybrid nanostructures enable achieving higher EFs due to the hotspots located at the interface between the metal (Au/Ag) and the semiconducting substrates (Si/ZnO), which potentially improve the detection limit. Moreover, a great reproducibility of SERS signal is obtained with these

hybrid nanosystems. Thus, a great number of hybrid nanostructures was carried out and employed as SERS substrates for obtaining high-performance sensors of different chemical/biological molecules with an excellent reliability and reproducibility.

During these two last decades, great progress has occurred in this research topic and a very small number of reviews concerning this progress can be found. Thus, an overview of these promising advances in the development of hybrid SERS nanosensors is presented. Firstly, we report on a review of the design and fabrication of hybrid SERS substrates based on silicon. Next, the representative results on the high sensitivity and the reproducibility of detection of chemical or biological molecules concerning these metal-coated Si SERS nanosensors are summarized. Lastly, a review on hybrid SERS substrates based on zinc oxide is reported concerning their fabrication and their SERS performances.

2. Hybrid SERS Nanosensors Based on Silicon Nanostructures

2.1. Fabrication Methods of Metal-Coated Si Nanosensors

Silicon nanostructures such as nanowires (SiNW) or nanopillars (SiNP) can mainly be obtained with the following fabrication methods, which are the solution phase synthesis (SPS) [45,46], the vapor–liquid–solid (VLS) growth [38,47–50], the oxide-assisted growth (OAG) [36,51,52], lithographic methods coupled to an etching process [53–55], and the metal-assisted chemical etching (MACE) [40,56,57] (see Figure 1a,b). More recently, a couple of techniques emerged such as maskless processes by reactive ion etching (RIE) [35] or RIE processes through the oxide native layer of silicon [58–60] (see Figure 1c). Moreover, a few groups employed a technique combining two existing techniques: the nanosphere lithography (NSL) and the MACE technique [61–64] (see Figure 1d for the principle scheme of this coupled technique of fabrication).

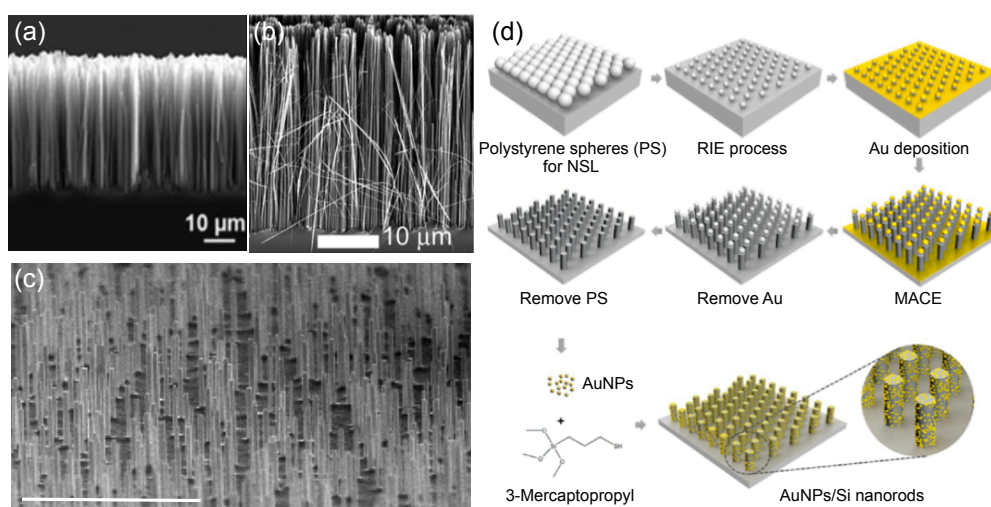


Figure 1. Three examples of metal-coated Si nanostructures (SEM images): (a) Si nanowires produced via a MACE technique (height $h = 24.3 \pm 1.9 \mu\text{m}$ and nanowire diameter: $50 \text{ nm} < D < 300 \text{ nm}$) coated with Ag nanoparticles (average AgNP diameter: $d = 30 \text{ nm}$), reproduced from [31] with permission from the Royal Society of Chemistry; (b) Si nanowires produced through an Ag-assisted chemical etching of n -Si(100) wafer (height $h \sim 32 \mu\text{m}$ and diameter: $80 \text{ nm} < D < 200 \text{ nm}$), reprinted with permission from [37], Copyright 2010 American Chemical Society; (c) Au/Si nanopillars (NP) obtained with the fabrication technique based on an RIE process through the oxide native layer followed by a deposition of a gold layer of 30 nm (scale bar = 5 μm , radius $R \sim 125 \text{ nm}$ and height $h \sim 1000 \text{ nm}$); (d) principle scheme of the low-cost fabrication process combining NSL and MACE for producing AuNP-conjugated Si nanorod arrays (reprinted with permission from [63], copyright 2017 American Chemical Society).

Thus, the SiNWs or SiNPs obtained with these various fabrication techniques are then modified with a metallic layer [35,58–60] or nanoparticles (e.g., Au and Ag nanoparticles) [31,36–39] in order to realize SERS substrates with significant performances in terms of the enhancement factor and the detection limit of biological and chemical molecules. The coating of Si nanostructures for SERS sensing is generally obtained with several Au nanostructures such as spherical nanoparticles, cylindrical nanorods, or triangular prisms [34]. Another technique employed for realizing metallic nanoparticles on silicon nanowires is the use of oxidation–reduction reactions, which consist of the reduction of metal ions by the electrons coming from the reaction on the SiNW surfaces etched by hydrofluoric acid [65]. These different metal-coated Si nanosensors have been fabricated in a major part at the wafer-scale [31,35,38,40,58–60,63].

2.2. SERS Performances of Metal-Coated Si Nanosystems for Chemical and Biological Sensing

In order to evaluate the SERS performances of metal-coated Si nanostructures for sensing of biological and chemical molecules, the enhancement factor (EF) is usually calculated. For that, two expressions are mainly employed. These two formulas giving EF and AEF (AEF = Analytical Enhancement Factor) are as follows:

$$EF = \frac{I_{SERS}}{I_{Raman}} \times \frac{N_{Raman}}{N_{SERS}}, \quad (1)$$

$$AEF = \frac{I_{SERS}}{I_{Raman}} \times \frac{C_{Raman}}{C_{SERS}}, \quad (2)$$

where I_{SERS} and I_{Raman} are SERS and Raman intensities for a given Raman peak, respectively. The N_{SERS} and N_{Raman} quantities are the numbers of excited molecules of analytes in SERS and Raman measurements, respectively. Finally, C_{SERS} and C_{Raman} correspond to concentrations of studied analytes used for SERS and Raman experiments, respectively. Firstly, the silicon nanowires coated with metallic nanoparticles demonstrated excellent SERS performances (see Table 1). For instance, Galopin et al. showed an EF factor in the range of 10^7 – 10^8 and a limit of detection (LOD) of 10 fM measured experimentally for the detection of Rhodamine 6G (R6G) molecules with Si nanowires coated with Ag nanoparticles [38] (see Figure 2a,b). With the same type of metal/Si systems (AgNPs/SiNWs), Zhang et al. obtained an EF factor in the range of 10^8 – 10^{10} for the detection of Sudan dyes [37]. Furthermore, an EF factor in the range of 6×10^9 – 8×10^9 is achieved and an LOD of 1 fM is experimentally measured for the DNA detection in the work of He et al. [36]. Besides, Wei et al. also demonstrated an LOD of 10 fM measured experimentally for the DNA sensing with Si nanowires coated with gold nanoparticles [33].

Secondly, the metal-coated Si nanosystems obtained with low-cost techniques also achieved great SERS performances for chemical and biological detection (see Table 1). Recently, Lin et al. fabricated Si nanorods with the coupling of the NSL and MACE techniques, and then coated these Si nanorods with gold nanoparticles (see Figures 1d and 2c,d). A value of 3×10^7 is achieved for the enhancement factor for the detection of Rhodamine 6G molecules [63] (see Figure 2d for SERS spectra). By using this technique of NSL associated with MACE, Cara et al. also showed a great EF of 1.6×10^6 for the detection of 7-mercapto-4-methylcoumarin (MMC) molecules with gold-coated Si nanowires [62]. With this same fabrication technique, Huang et al. achieved an EF of 1.1×10^6 for the detection of 4-aminothiophenol (4-AT) molecules with silver-coated Si nanowires [66]. By another way, Schmidt et al. demonstrated an EF value of 7×10^6 for the detection of trans-1,2-bis(4-pyridyl)ethylene (BPE) with leaning Ag-coated Si nanopillars. These nanosystems have been produced with a maskless process by using reactive ion etching. By leaning the Ag/Si nanopillars, hotspots are created and thus improving the Raman signal enhancement [35].

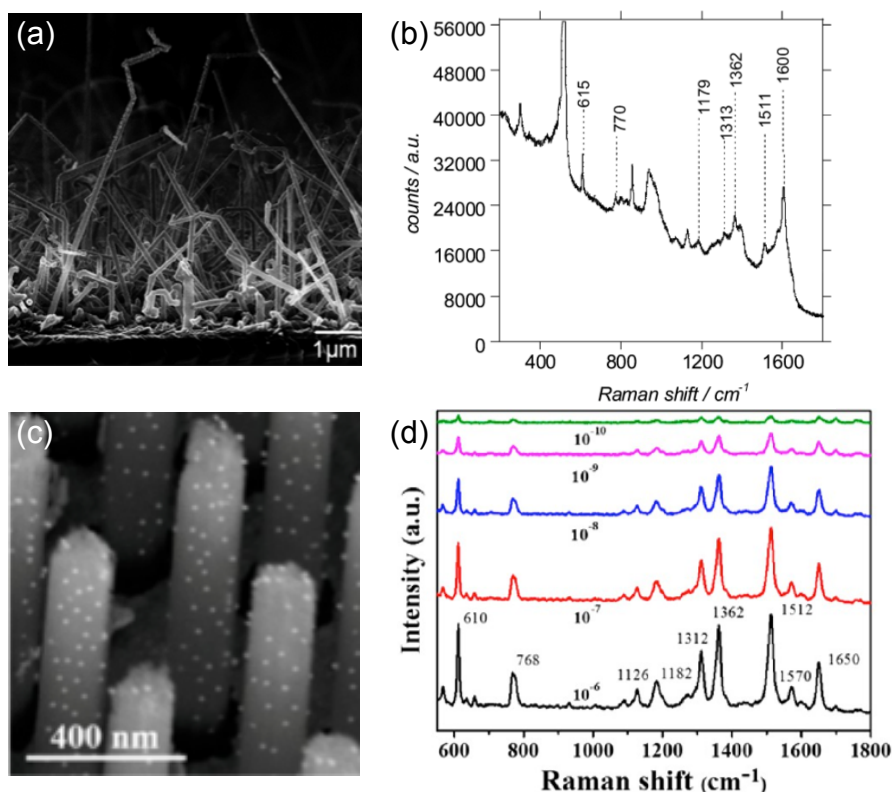


Figure 2. (a) Si nanowires produced by the vapor–liquid–solid growth (height: $5 \mu\text{m} < h < 6 \mu\text{m}$ and nanowire diameter: $50 \text{ nm} < D < 150 \text{ nm}$) coated with Ag nanoparticles (diameter: $4 \text{ nm} < d < 40 \text{ nm}$); (b) SERS spectrum of Rhodamine 6G (R6G) molecules ($C_{R6G} = 10^{-9} \text{ M}$) adsorbed on AgNPs/SiNWs. (a,b) are reprinted with permission from [38], copyright 2009 American Chemical Society; (c) Si nanorod array obtained with the combination of the NSL and MACE techniques followed by the grafting of gold nanoparticles having a diameter of 20 nm on Si nanorods (period $P \sim 500 \text{ nm}$ between two Si nanorods, diameter $D \sim 200 \text{ nm}$ and height $h \sim 1300 \text{ nm}$); (d) SERS spectra of R6G molecules adsorbed on AuNPs/SiNRs for concentrations varying from 10^{-10} to 10^{-6} M ; (c,d) are reprinted with permission from [63], copyright 2017 American Chemical Society.

Table 1. SERS performances of metal-coated Si nanosystems for chemical and biological sensing.

SERS Substrates	Detected Molecules	EF or AEF	LOD (M)	RSD	Refs.
AgNPs/SiNWs	R6G	10^7 – 10^8	10^{-14}	–	[38]
AgNPs/SiNWs	Sudan Dyes	10^8 – 10^{10}	–	<30%	[37]
AgNPs/SiNWs	MB	10^6 – 4×10^6	–	<10%	[31]
AgNPs/SiNWs	DNA	6×10^9 – 8×10^9	10^{-15}	–	[36]
Ag/SiNWs	Calcium Dipicolinate	–	4×10^{-6}	<20%	[40]
Ag/SiNWs	4-AT	1.1×10^6	–	<15%	[66]
AuNPs/SiNWs	DNA	–	10^{-14}	<10%	[33]
Au/SiNWs	MMC	1.6×10^6	–	<20%	[62]
AuNPs/SiNRs	R6G	3×10^7	10^{-10}	<8%	[63]
Leaning Ag/SiNPs	BPE	7×10^6	–	~10%	[35]
Au/SiNPs	Thiophenol	10^7 – 10^8	–	<7%	[58]
Al/SiNPs	Thiophenol	1.5×10^7 – 2.5×10^7	–	<7%	[60]

AgNPs = Ag nanoparticles; AuNPs = Au nanoparticles; Au or Ag or Al = metallic layer; SiNWs = Si nanowires; SiNRs = Si nanorods; SiNPs = Si nanopillars, and RSD = Relative Standard Deviation for SERS intensity.

In addition, Prof. Barbillon's group demonstrated excellent enhancement factors (EF or AEF) for the detection of thiophenol molecules with Au/Si and Al/Si nanopillars. For these two cases, Si nanopillars have been produced by a RIE process through the oxide native layer of silicon followed by the evaporation of a metallic layer. The values achieved for EF (for Au/Si) and AEF (for Al/Si) are in the range 10^7 – 10^8 [58] and 1.5×10^7 – 2.5×10^7 [60], respectively. Furthermore, this group also showed that the thickness of the metallic layer (for gold) has an effect on the SERS enhancement [59]. Lastly, other groups also demonstrated SERS enhancements with other shapes of Si nanosystems such as a tip-shaped silicon metasurface coated with gold nanoparticles [67,68], a hybrid Si nanospheroid network ornamented with gold nanospheres [69], silver-coated Si nanopores [70], or Si nanowire arrays coated silver nanoparticles [71,72]. To conclude Section 2, the interests of the metal-coated Si nanosystems are the use of fabrication techniques known as large-surface techniques, and also the plasmonic coupling between the metallic layer/nanoparticles and the semiconducting silicon substrate [38,58,73] in order to potentially improve the Raman enhancement. Moreover, a great reproducibility of the SERS signal is achieved with both metal-coated Si nanosystems produced with the techniques previously cited (average RSD = 15%, see Table 1). The Relative Standard Deviations for the SERS intensity of the studied Raman peaks are calculated on the basis of several SERS spectra recorded on different locations of each SERS substrate studied here. Nonetheless, some of these fabrication techniques are expensive and time consuming for a mass production. Finally, EF values obtained with the metal-coated Si nanosensors are higher or equal to more conventional SERS substrates such as core-shell nanosphere dimers (EF = 10^5 – 5×10^7 for Au-SiO₂ or Au-Pt nanosphere dimer) [74,75], a bare Au nanosphere dimer on a Si surface and on Pt surface (EF = 10^5 – 9×10^7) [74,76], or Au nanoparticles with a silver coating (EF = 10^4 – 10^5) [77].

3. Hybrid SERS Nanosensors Based on Zinc Oxide Nanostructures

3.1. Fabrication Methods of Metal-Coated ZnO Nanosensors

To produce metal-coated ZnO nanosystems, several techniques can be employed. At first, this begins by the fabrication of ZnO nanostructures by using various growth techniques such as the pulsed-laser deposition (PLD) [44,78–80], the hydrothermal growth [42,43,81] (see Figures 3a,b and 4a,c), the vapor-liquid-solid (VLS) or vapor-solid (VS) growth [41,82–84] (see Figure 5b). Then, after this step, metallic nanoparticles or a metallic layer are added with different techniques such as a sputtering process [41–43], an electron beam evaporation [44], a hydrothermal method [85], a controlled wet chemistry method associated with a spin-coater [86], a photochemical deposition method [81,87], and a dip-coating process [82]. In addition, a low-cost and wafer-scale technique based on NSL and solution processes has been developed by He et al. (see Figure 3d for the principle scheme of this fabrication method) for producing, for instance, urchin-like Ag nanoparticle/ZnO hollow nanosphere arrays (see Figure 3c) [88]. These different metal-coated ZnO nanosensors have been realized in a major part at the wafer-scale [41–43,85,86].

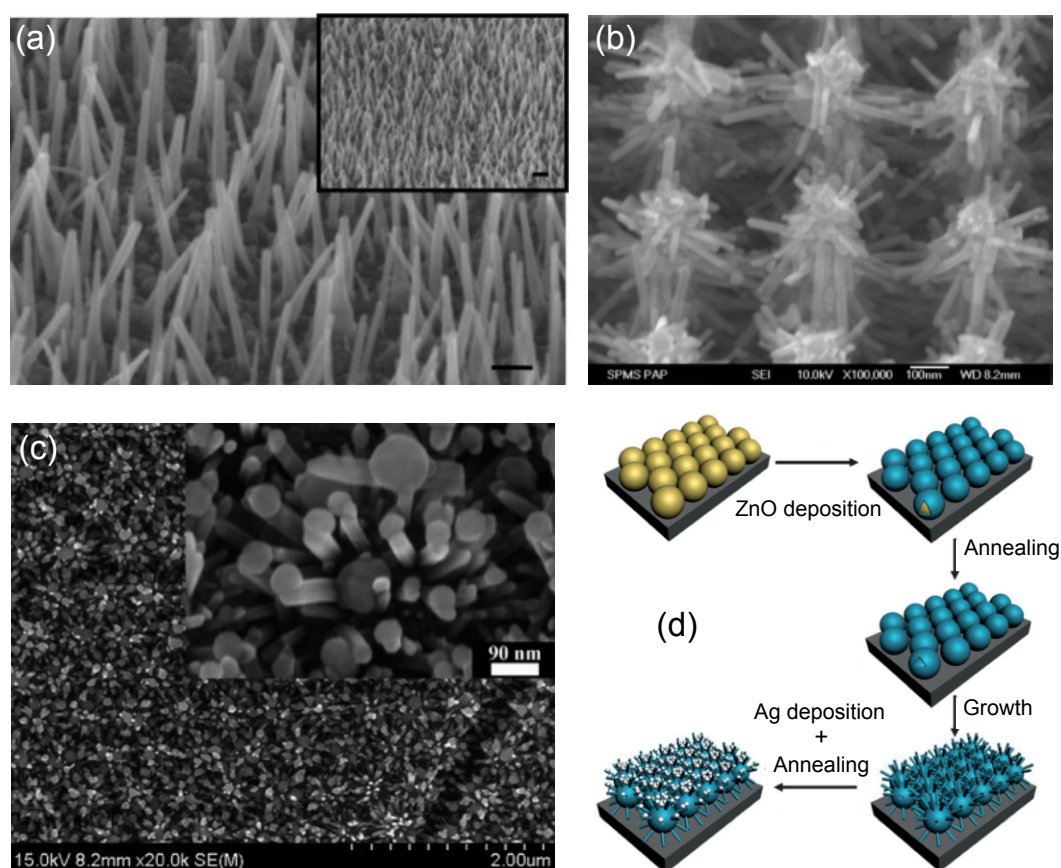


Figure 3. Three examples of metal-coated ZnO nanostructures: (a) SEM images of Au/ZnO nanorods and the insert is a picture at a weaker magnification (scale bars = 100 nm; reprinted with permission from [42], copyright 2011 American Chemical Society); (b) SEM image of AgNP-decorated Si/ZnO nanotrees (scale bar = 100 nm; reprinted with permission from [81], copyright 2010 American Chemical Society); (c) SEM images of an urchin-like AgNPs/ZnO hollow nanosphere (HNS) array and the insert corresponds to a picture recorded with a higher magnification; (d) principle scheme of the low-cost fabrication process of urchin-like AgNPs/ZnO HNS array; (c,d) are reproduced from [88] with permission from the Royal Society of Chemistry.

3.2. SERS Performances of Metal-Coated ZnO Nanosystems for Chemical Sensing

As previously, to evaluate the SERS performances of metal/ZnO nanostructures for sensing of chemical molecules, the enhancement factor (EF) is usually calculated by using one of the two equations Equations (1) and (2), and sometimes a formula of the SERS gain (G_{SERS}) is also used:

$$G_{SERS} = \frac{I_{SERS}}{I_{Raman}}, \quad (3)$$

where I_{SERS} and I_{Raman} are SERS and Raman intensities for a given Raman peak, respectively. Firstly, the zinc oxide nanostructures coated with gold nanoparticles or a gold layer demonstrated excellent SERS performances (see Table 2). For instance, Chen et al. demonstrated an excellent EF of 1.2×10^7 obtained with Rhodamine 6G (R6G) molecules by using Au/ZnO nanoneedles (see Figure 4a,b). They also showed that the EF value depended on the density of gold nanoparticles and the morphology of Au/ZnO nanoneedles [85]. Another interesting example is those of Sinha et al. where zinc oxide nanorods have been coated with a gold layer, and a limit of detection (LOD) in terms of concentration was experimentally found and equals 1 pM for methylene blue (MB) molecules. They also demonstrated a good reproducibility of the SERS signal before each cleaning cycle assisted

by UV [42]. Other groups observed different effects on the SERS signal such as the metal thickness [41], the density of gold/ZnO nanostructures [44] and the renewability of the gold/ZnO substrates [87,89]. Secondly, the zinc oxide nanostructures coated with Ag nanoparticles or a silver layer also showed great SERS performances (see Table 2). For example, Cui et al. showed a great EF evaluated at 2.5×10^{10} and an LOD of 1 pM measured experimentally for Malachite green (MG) molecules by using ZnO nanowire arrays coated with Ag nanoparticles (see Figure 4c,d). A low concentration of amoxicillin (1 nM) has been also experimentally detected with these Ag/ZnO nanostructures [43]. Furthermore, He et al. obtained great SERS performances for the detection of Rhodamine 6G molecules with urchin-like Ag nanoparticle/ZnO hollow nanosphere arrays. An EF of 10^8 is found and an LOD of 10^{-10} M is experimentally measured. They demonstrated that the SERS enhancement came from the great density of hotspots created by the multi-AgNP decoration, the charge transfer between Ag and ZnO, and the plasmonic coupling between AgNPs [88]. In another way, Song et al. observed a great EF of 1.2×10^8 and experimentally measured an LOD of 1 pM for *p*-aminothiophenol (PATP) molecules with ZnO nanofibers deposited on a silver foil surface. They demonstrated that SERS enhancement came from the exciton–plasmon interactions between ZnO nanofibers and the Ag foil surface, and also the fact that this type of Ag/ZnO nanosystem has a great photocatalytic activity towards pollutant (in this example, methylene blue (MB) molecules) degradation under UV illumination [90].

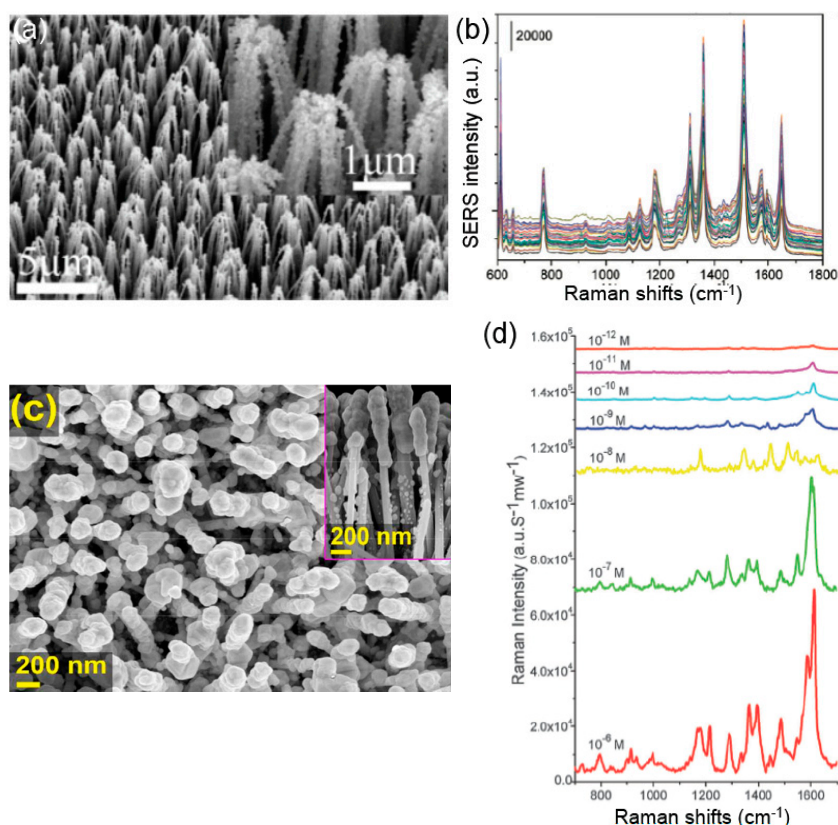


Figure 4. (a) SEM images of Au/ZnO nanoneedles and the insert is a zoom on a couple of nanoneedles; (b) SERS spectra of R6G molecules ($C_{R6G} = 10^{-7}$ M) adsorbed on Au/ZnO nanoneedles. (a,b) are reprinted with permission from [85], copyright 2010 American Chemical Society; (c) SEM images of Ag/ZnO nanowire array (NWA) and the insert corresponds to the cross-section of this array; (d) SERS spectra of MG molecules adsorbed on Ag/ZnO NWA for different MG concentrations; (c,d) are reproduced from [43] with permission from the Royal Society of Chemistry.

Table 2. SERS performances of metal-coated ZnO nanosystems for chemical sensing.

SERS Substrates	Detected Molecules	EF/AEF/G _{SERS}	LOD (M)	RSD	Refs.
Au/ZnO-NWs	4-MBT	2.2×10^6	–	<10%	[41]
Au/ZnO nanoneedles	R6G	1.2×10^7	–	<15%	[85]
Au/ZnO-NRs	MB	–	10^{-12}	–	[42]
Au/ZnO Inverse Nanostructures	Thiophenol	1.4×10^5	–	<20%	[89]
AuNPs/ZnO-NRs (Dendritic)	R6G	–	10^{-9}	–	[87]
Au/ZnO-NPs	Thiophenol	24	–	7%–45%	[44]
AuNPs/Ag/ZnO-Nanocones	Thiophenol	10^{10} – 10^{11}	10^{-19}	–	[82]
AgNPs/Ag/ZnO-NWs	MG	2.5×10^{10}	10^{-12}	–	[43]
AgNPs/Si/ZnO nanotrees	R6G	10^6	–	<20%	[81]
AgNPs/wheatear-like H-ZnO	R6G	4.9×10^7	10^{-9}	<15%	[86]
AgFoil/ZnO nanofibers	PATP	1.2×10^8	10^{-12}	–	[90]
AgNPs/urchin-like ZnO-HNS	R6G	10^8	10^{-10}	<20%	[88]
AgNPs/ZnO-Nanoworms	R6G	3.1×10^7	10^{-10}	–	[91]
AgNPs/ZnO-NRs	4-ATP	2×10^6	–	–	[92]

AgNPs = Ag Nanoparticles; Au = metallic layer; ZnO-NWs = ZnO Nanowires; ZnO-NRs = ZnO Nanorods, H-ZnO = Hydrogenated ZnO, ZnO-NPs = ZnO Nanopillars, ZnO-HNS = ZnO Hollow Nanospheres, and RSD = Relative Standard Deviation for SERS intensity.

Several groups also demonstrated interesting properties for the Ag/ZnO nanosystems such as the superhydrophobicity [91], the hydrogenation of ZnO for improving the SERS enhancement [86], and their integration in microfluidic systems [92]. Finally, a couple of groups observed excellent EF with AgNPs/Si/ZnO and AuNPs/Ag/ZnO nanosystems. Indeed, Cheng et al. achieved an EF of 10^6 with Rhodamine 6G molecules by using AgNPs/Si/ZnO nanotrees [81], and Lee et al. an EF of 10^{10} – 10^{11} and an LOD of 10^{-19} M which was experimentally measured with thiophenol molecules by using AuNPs/Ag/ZnO nanocones (see Figure 5). With this original design, Lee et al. obtained significant improvements of the SERS signal by using both following properties: the light trapping thanks to the nanocone arrays with a graded refractive index, the effect of plasmonic waveguide obtained with Ag-coated nanocones, and gap plasmons between AuNPs and Ag film (see Figure 5a) [82].

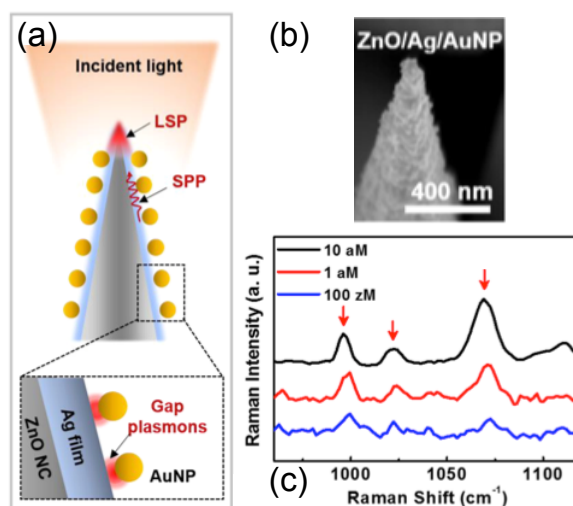


Figure 5. (a) scheme of the detection principle of SERS nanosensor (Electric field located at the tip and at the particle–film gap; SPP = Surface Plasmon Polariton and LSP = Localized Surface Plasmon); (b) SEM image of an AuNPs/Ag/ZnO nanocone; (c) SERS spectra of thiophenol molecules adsorbed on AuNPs/Ag/ZnO nanocones at the trace level (for three very low concentrations). All are reprinted with permission from [82], copyright 2015 American Chemical Society.

To conclude Section 3, the interests of the metal-coated ZnO nanosystems are mainly the use of low-cost fabrication techniques, the plasmonic coupling between the metallic layer/nanoparticles and the semiconducting substrate, and also the plasmonic coupling of metallic nanoparticles in order to potentially improve the Raman enhancement. Moreover, a good reproducibility of the SERS signal is also achieved with both metal-coated ZnO nanosystems fabricated by the techniques previously cited (average RSD = 20%, see Table 2). As for metal-coated Si nanosystems, the RSD values concerning the SERS intensity of the studied Raman peaks are calculated on the basis of several SERS spectra recorded at different locations of each SERS substrate studied here. Finally, EF values obtained with the metal-coated ZnO nanosensors are higher or equal to more conventional SERS substrates such as core-shell nanosphere dimers ($EF = 10^5\text{--}5 \times 10^7$ for Au-SiO₂ or Au-Pt nanosphere dimer) [74,75], a bare Au nanosphere dimer on a Si surface and on Pt surface ($EF = 10^5\text{--}9 \times 10^7$) [74,76], or Au nanoparticles with a silver coating ($EF = 10^4\text{--}10^5$) [77].

4. Conclusions

In this short review, recent advances are presented concerning the development and the performances of SERS nanosensors based Si or ZnO nanostructures coated with a metallic layer or metallic nanoparticles for a very sensitive and reproducible detection of chemical and biological molecules. These metal-coated semiconducting SERS nanosensors highlighted excellent EF values and a great reproducibility with an average RSD of 15% and 20%, respectively, as described in the second and third sections. These two types of nanosensors can be produced with low-cost and wafer-scale techniques that have recently been developed. Thus, all these advances can enable an application of these SERS nanosensors to industrial and practical domains by using them as reliable, powerful and robust analytical platforms in the near future. However, a great number of works need to be conducted in order to better understand all the mechanisms involved in such metal-coated semiconducting nanostructures for enhancing the Raman signal. Furthermore, the hybrid metal-coated zinc oxide nanosystems can be used for applications to plasmonic photocatalysis thanks to the great photocatalytic efficiency of zinc oxide [93,94].

Funding: This research received no external funding.

Conflicts of Interest: The author declares no conflict of interest.

References

1. Yan, J.; Han, X.; He, J.; Kang, L.; Zhang, B.; Du, Y.; Zhao, H.; Dong, C.; Wang, H.-L.; Xu, P. Highly sensitive surface-enhanced Raman spectroscopy (SERS) platforms based on silver nanostructures fabricated on polyaniline membrane surfaces. *ACS Appl. Mater. Interfaces* **2012**, *4*, 2752–2756. [[CrossRef](#)] [[PubMed](#)]
2. Li, S.; Xu, P.; Ren, Z.; Zhang, B.; Du, Y.; Han, X.; Mack, N.H.; Wang, H.-L. Fabrication of thorny Au nanostructures on polyaniline surfaces for sensitive surface-enhanced Raman spectroscopy. *ACS Appl. Mater. Interfaces* **2013**, *5*, 49–54. [[CrossRef](#)] [[PubMed](#)]
3. Bodelon, G.; Montes-Garcia, V.; Lopez-Puente, V.; Hill, E.H.; Hamon, C.; Sanz-Ortiz, M.N.; Rodal-Cedeira, S.; Costas, C.; Celiksoy, S.; Perez-Juste, I.; et al. Detection and imaging of quorum sensing in *Pseudomonas aeruginosa* biofilm communities by surface-enhanced resonance Raman scattering. *Nat. Mater.* **2016**, *15*, 1203–1211. [[CrossRef](#)] [[PubMed](#)]
4. Sharma, B.; Cardial, M.F.; Kleinman, S.L.; Greeneltch, N.G.; Frontiera, R.R.; Blaber, M.G.; Schatz, G.C.; Van Duyne, R.P. High-performance SERS substrates: Advances and challenges. *MRS Bull.* **2013**, *38*, 615–624. [[CrossRef](#)]
5. Jimenez de Aberasturi, D.; Serano-Montes, A.B.; Langer, J.; Henriksen-Lacey, M.; Parak, W.J.; Liz-Marzan, L.M. Surface enhanced Raman scattering encoded gold nanostars for multiplexed cell discrimination. *Chem. Mater.* **2016**, *28*, 6779–6790. [[CrossRef](#)]
6. Rodriguez-Fernandez, D.; Langer, J.; Henriksen-Lacey, M.; Liz-Marzan, L.M. Hybrid Au-SiO₂ core-satellite colloids as switchable SERS tags. *Chem. Mater.* **2015**, *27*, 2540–2545. [[CrossRef](#)]

7. La Porta, A.; Sanchez-Iglesias, A.; Altantzis, T.; Bals, S.; Grzelczak, M.; Liz-Marzan, L.M. Multifunctional self-assembled composite colloids and their application to SERS detection. *Nanoscale* **2015**, *7*, 10377–10381. [[CrossRef](#)]
8. Wang, Q.; Lu, G.; Hou, L.; Zhang, T.; Luo, C.; Yang, H.; Barbillon, G.; Lei, F.H.; Marquette, C.A.; Perriat, P.; et al. Fluorescence correlation spectroscopy near individual gold nanoparticle. *Chem. Phys. Lett.* **2011**, *503*, 256–261. [[CrossRef](#)]
9. Dalstein, L.; Ben Haddada, M.; Barbillon, G.; Humbert, C.; Tadjeddine, A.; Boujday, S.; Busson, B. Revealing the interplay between adsorbed molecular layers and gold nanoparticles by linear and nonlinear optical properties. *J. Phys. Chem. C* **2015**, *119*, 17146–17155. [[CrossRef](#)]
10. Yu, Q.; Guan, P.; Qin, D.; Golden, G.; Wallace, P.M. Inverted size-dependence of surface-enhanced Raman scattering on gold nanohole and nanodisk arrays. *Nano Lett.* **2008**, *8*, 1923–1928. [[CrossRef](#)]
11. Faure, A.-C.; Barbillon, G.; Ou, M.; Ledoux, G.; Tillement, O.; Roux, S.; Fabregue, D.; Descamps, A.; Bijeon, J.-L.; Marquette, C.A.; et al. Core/shell nanoparticles for multiple biological detection with enhanced sensitivity and kinetics. *Nanotechnology* **2008**, *19*, 485103. [[CrossRef](#)] [[PubMed](#)]
12. Barbillon, G.; Faure, A.-C.; El Kork, N.; Moretti, P.; Roux, S.; Tillement, O.; Ou, M.G.; Descamps, A.; Perriat, P.; Vial, A.; et al. How nanoparticles encapsulating fluorophores allow a double detection of biomolecules by localized surface plasmon resonance and luminescence. *Nanotechnology* **2008**, *19*, 035705. [[CrossRef](#)] [[PubMed](#)]
13. Zhang, P.; Yang, S.; Wang, L.; Zhao, J.; Zhu, Z.; Liu, B.; Zhong, J.; Sun, X. Large-scale uniform Au nanodisk arrays fabricated via X-ray interference lithography for reproducible and sensitive SERS substrate. *Nanotechnology* **2014**, *25*, 245301. [[CrossRef](#)] [[PubMed](#)]
14. Barbillon, G.; Bijeon, J.-L.; Lérondel, G.; Plain, J.; Royer, P. Detection of chemical molecules with integrated plasmonic glass nanotips. *Surf. Sci.* **2008**, *602*, L119–L122. [[CrossRef](#)]
15. Ahn, H.-J.; Thiyagarajan, P.; Jia, L.; Kim, S.-I.; Yoon, J.-C.; Thomas, E.L.; Jang, J.-H. An optimal substrate design for SERS: Dual-scale diamond-shaped gold nano-structures fabricated via interference lithography. *Nanoscale* **2013**, *5*, 1836–1842. [[CrossRef](#)]
16. Vo-Dinh, T.; Dhawan, A.; Norton, S.J.; Khoury, C.G.; Wang, H.N.; Misra, V.; Gerhold, M.D. Plasmonic nanoparticles and nanowires: Design, fabrication and application in sensing. *J. Phys. Chem. C* **2010**, *114*, 7480–7488. [[CrossRef](#)] [[PubMed](#)]
17. Dhawan, A.; Duval, A.; Nakkach, M.; Barbillon, G.; Moreau, J.; Canva, M.; Vo-Dinh, T. Deep UV nano-microstructuring of substrates for surface plasmon resonance imaging. *Nanotechnology* **2011**, *22*, 165301. [[CrossRef](#)]
18. Gillibert, R.; Sarkar, M.; Bryche, J.-F.; Yasukuni, R.; Moreau, J.; Besbes, M.; Barbillon, G.; Bartenlian, B.; Canva, M.; Lamy de la Chapelle, M. Directional surface enhanced Raman scattering on gold nano-gratings. *Nanotechnology* **2016**, *27*, 115202. [[CrossRef](#)]
19. Bryche, J.-F.; Gillibert, R.; Barbillon, G.; Sarkar, M.; Coutrot, A.-L.; Hamouda, F.; Aassime, A.; Moreau, J.; Lamy de la Chapelle, M.; Bartenlian, B.; et al. Density effect of gold nanodisks on the SERS intensity for a highly sensitive detection of chemical molecules. *J. Mater. Sci.* **2015**, *50*, 6601–6607. [[CrossRef](#)]
20. Bryche, J.-F.; Gillibert, R.; Barbillon, G.; Gogol, P.; Moreau, J.; Lamy de la Chapelle, M.; Bartenlian, B.; Canva, M. Plasmonic enhancement by a continuous gold underlayer: Application to SERS sensing. *Plasmonics* **2016**, *11*, 601–608. [[CrossRef](#)]
21. Bryche, J.-F.; Tsigara, A.; Bélier, B.; Lamy de la Chapelle, M.; Canva, M.; Bartenlian, B.; Barbillon, G. Surface enhanced Raman scattering improvement of gold triangular nanoprisms by a gold reflective underlayer for chemical sensing. *Sens. Actuator B* **2016**, *228*, 31–35. [[CrossRef](#)]
22. Masson, J.-F.; Gibson, K.F.; Provencher-Girard, A. Surface-enhanced Raman spectroscopy amplification with film over etched nanospheres. *J. Phys. Chem. C* **2010**, *114*, 22406–22412. [[CrossRef](#)]
23. Camden, J.P.; Dieringer, J.A.; Zhao, J.; Van Duyne, R.P. Controlled plasmonic nanostructures for surface-enhanced spectroscopy and sensing. *Acc. Chem. Res.* **2008**, *41*, 1653–1661. [[CrossRef](#)] [[PubMed](#)]
24. Hamouda, F.; Sahaf, H.; Held, S.; Barbillon, G.; Gogol, P.; Moyon, E.; Aassime, A.; Moreau, J.; Canva, M.; Lourtioz, J.-M.; et al. Large area nanopatterning by combined anodic aluminum oxide and soft UV-NIL technologies for applications in biology. *Microelectron. Eng.* **2011**, *88*, 2444–2446. [[CrossRef](#)]

25. Cottat, M.; Lidgi-Guigui, N.; Tijunelyte, I.; Barbillon, G.; Hamouda, F.; Gogol, P.; Aassime, A.; Lourtioz, J.-M.; Bartenlian, B.; Lamy de la Chapelle, M. Soft UV nanoimprint lithography-designed highly sensitive substrates for SERS detection. *Nanoscale Res. Lett.* **2014**, *9*, 623. [[CrossRef](#)] [[PubMed](#)]
26. Jahn, M.; Patze, S.; Hidi, I.J.; Knipper, R.; Radu, A.I.; Mühling, A.; Yüksel, S.; Peksa, V.; Weber, K.; Mayerhöfer, T.; et al. Plasmonic nanostructures for surface enhanced spectroscopic methods. *Analyst* **2016**, *141*, 756–793. [[CrossRef](#)] [[PubMed](#)]
27. Que, R.; Shao, M.; Zhuo, S.; Wen, C.; Wang, S.; Lee, S.-T. Highly reproducible surface-enhanced Raman scattering on a capillarity-assisted gold nanoparticle assembly. *Adv. Funct. Mater.* **2011**, *21*, 3337–3343. [[CrossRef](#)]
28. Tanoue, Y.; Sugawa, K.; Yamamuro, T.; Akiyama, T. Densely arranged two-dimensional silver nanoparticle assemblies with optical uniformity over vast areas as excellent surface-enhanced Raman scattering substrates. *Phys. Chem. Chem. Phys.* **2013**, *15*, 15802–15805. [[CrossRef](#)]
29. Sugawa, K.; Akiyama, T.; Tanoue, Y.; Harumoto, T.; Yanagida, S.; Yasumori, A.; Tomita, S.; Otsuki, J. Particle size dependence of the surface-enhanced Raman scattering properties of densely arranged two-dimensional assemblies of Au(core)–Ag(shell) nanospheres. *Phys. Chem. Chem. Phys.* **2015**, *17*, 21182–21189.
30. Convertino, A.; Mussi, V.; Maiolo, L. Disordered array of Au covered silicon nanowires for SERS biosensing combined with electrochemical detection. *Sci. Rep.* **2016**, *6*, 25099. [[CrossRef](#)]
31. Akin, M.S.; Yilmaz, M.; Babur, E.; Ozdemur, B.; Erdogan, H.; Tamer, U.; Demirel, G. Large area uniform deposition of silver nanoparticles through bio-inspired polydopamine coating on silicon nanowire arrays for practical SERS applications. *J. Mater. Chem. B* **2014**, *2*, 4894–4900. [[CrossRef](#)]
32. Wang, H.; Jiang, X.; Lee, S.T.; He, Y. Silicon nanohybrid-based surface-enhanced Raman scattering sensors. *Small* **2014**, *10*, 4455–4468. [[CrossRef](#)] [[PubMed](#)]
33. Wei, X.P.; Su, S.; Guo, Y.Y.; Jiang, X.X.; Zhong, Y.L.; Su, Y.Y.; Fan, C.H.; Lee, S.T.; He, Y. A molecular beacon-based signal-off surface-enhanced Raman scattering strategy for highly sensitive, reproducible, and multiplexed DNA detection. *Small* **2013**, *9*, 2493–2499. [[CrossRef](#)] [[PubMed](#)]
34. Chen, R.; Li, D.; Hu, H.; Zhao, Y.; Wang, Y.; Wong, N.; Wang, S.; Zhang, Y.; Hu, J.; Shen, Z.; et al. Tailoring optical properties of silicon nanowires by Au nanostructure decorations: Enhanced Raman scattering and photodetection. *J. Phys. Chem. C* **2012**, *116*, 4416–4422. [[CrossRef](#)]
35. Schmidt, M.S.; Hübner, J.; Boisen, A. Large area fabrication of leaning silicon nanopillars for surface enhanced Raman spectroscopy. *Adv. Mater.* **2012**, *24*, OP11–OP18. [[CrossRef](#)] [[PubMed](#)]
36. He, Y.; Su, S.; Xu, T.T.; Zhong, Y.L.; Zapien, J.A.; Li, J.; Fan, C.H.; Lee, S.T. Silicon nanowires-based highly-efficient SERS-active platform for ultrasensitive DNA detection. *Nano Today* **2011**, *6*, 122–130. [[CrossRef](#)]
37. Zhang, M.L.; Fan, X.; Zhou, H.W.; Shao, M.W.; Antonio Zapien, J.; Wong, N.B.; Lee, S.T. A high-efficiency surface-enhanced Raman scattering substrate based on silicon nanowires array decorated with silver nanoparticles. *J. Phys. Chem. C* **2010**, *114*, 1969–1975. [[CrossRef](#)]
38. Galopin, E.; Barbillat, J.; Coffinier, Y.; Szunerits, S.; Patriarche, G.; Boukherroub, R. Silicon nanowires coated with silver nanostructures as ultrasensitive interfaces for surface-enhanced Raman spectroscopy. *ACS Appl. Mater. Interfaces* **2009**, *1*, 1396–1403. [[CrossRef](#)]
39. Chen, J.; Martensson, T.; Dick, K.A.; Deppert, K.; Xu, H.Q.; Samuelson, L.; Xu, H. Surface-enhanced Raman scattering of rhodamine 6G on nanowire arrays decorated with gold nanoparticles. *Nanotechnology* **2008**, *19*, 275712. [[CrossRef](#)]
40. Zhang, B.H.; Wang, H.S.; Lu, L.H.; Ai, K.L.; Zhang, G.; Cheng, X.L. Large-area silver-coated silicon nanowire arrays for molecular sensing using surface-enhanced Raman spectroscopy. *Adv. Funct. Mater.* **2008**, *18*, 2348–2355. [[CrossRef](#)]
41. Khan, M.A.; Hogan, T.P.; Shanker, B. Gold-coated zinc oxide nanowire-based substrate for surface-enhanced Raman spectroscopy. *J. Raman Spectrosc.* **2009**, *40*, 1539–1545. [[CrossRef](#)]
42. Sinha, G.; Depero, L.E.; Alessandri, I. Recyclable SERS substrates based on Au-coated ZnO nanorods. *ACS Appl. Mater. Interfaces* **2011**, *3*, 2557–2563. [[CrossRef](#)] [[PubMed](#)]
43. Cui, S.; Dai, Z.; Tian, Q.; Liu, J.; Xiao, X.; Jiang, C.; Wu, W.; Roy, V.A.L. Wetting properties and SERS applications of ZnO/Ag nanowire arrays patterned by a screen printing method. *J. Mater. Chem. C* **2016**, *4*, 6371–6379. [[CrossRef](#)]
44. Barbillon, G.; Sandana, V.E.; Humbert, C.; Bélier, B.; Rogers, D.J.; Teherani, F.H.; Bove, P.; McClintock, R.; Razeghi, M. Study of Au coated ZnO nanoarrays for surface enhanced Raman scattering chemical sensing. *J. Mater. Chem. C* **2017**, *5*, 3528–3535. [[CrossRef](#)]

45. Holmes, J.D.; Johnston, K.P.; Doty, R.C.; Korgel, B.A. Control of thickness and orientation of solution-grown silicon nanowires. *Science* **2000**, *287*, 1471–1473. [[CrossRef](#)]
46. Tuan, H.Y.; Lee, D.C.; Hanrath, T.; Korgel, B.A. Catalytic solid-phase seeding of silicon nanowires by nickel nanocrystals in organic solvents. *Science* **2005**, *5*, 681–684. [[CrossRef](#)] [[PubMed](#)]
47. Hochbaum, A.I.; Fan, R.; He, R.; Yang, P. Controlled growth of Si nanowire arrays for device integration. *Nano Lett.* **2005**, *5*, 457–460. [[CrossRef](#)]
48. Kayes, B.M.; Filler, M.A.; Putnam, M.C.; Kelzenberg, M.D.; Lewis, N.S.; Atwater, H.A. Growth of vertically aligned Si wire arrays over large areas (>1 cm²) with Au and Cu catalysts. *Appl. Phys. Lett.* **2007**, *91*, 103110. [[CrossRef](#)]
49. Putnam, M.C.; Filler, M.A.; Kayes, B.M.; Kelzenberg, M.D.; Guan, Y.; Lewis, N.S.; Eiler, J.M.; Atwater, H.A. Secondary ion mass spectrometry of vapor–liquid–solid grown, Au-catalyzed, Si wires. *Nano Lett.* **2008**, *8*, 3109–3113. [[CrossRef](#)]
50. Schmidt, V.; Wittemann, J.; Gosele, U. Growth, thermodynamics, and electrical properties of silicon nanowires. *Chem. Rev.* **2010**, *110*, 361–388. [[CrossRef](#)]
51. Lee, S.T.; Wang, N.; Zhang, Y.F.; Tang, Y.H. Oxide-assisted semiconductor nanowire growth. *MRS Bull.* **1999**, *24*, 36–42. [[CrossRef](#)]
52. Ma, D.D.D.; Lee, C.S.; Au, F.C.K.; Tong, S.Y.; Lee, S.T. Small-diameter silicon nanowire surfaces. *Science* **2003**, *299*, 1874–1877. [[CrossRef](#)] [[PubMed](#)]
53. Caldwell, J.D.; Glembocki, O.; Bezares, F.J.; Bassim, N.D.; Rendell, R.W.; Feygelson, M.; Ukaegbu, M.; Kasica, R.; Shirey, L.; Hosten, C. Plasmonic nanopillar arrays for large-area, high-enhancement surface-enhanced Raman scattering sensors. *ACS Nano* **2011**, *5*, 4046–4055. [[CrossRef](#)] [[PubMed](#)]
54. Juhasz, R.; Elfstrom, N.; Linnros, J. Controlled fabrication of silicon nanowires by electron beam lithography and electrochemical size reduction. *Nano Lett.* **2005**, *5*, 275–280. [[CrossRef](#)] [[PubMed](#)]
55. Khorasaninejad, M.; Walia, J.; Saini, S.S. Enhanced first-order Raman scattering from arrays of vertical silicon nanowires. *Nanotechnology* **2012**, *23*, 275706. [[CrossRef](#)] [[PubMed](#)]
56. Peng, K.Q.; Hu, J.J.; Yan, Y.J.; Wu, Y.; Fang, H.; Xu, Y.; Lee, S.T.; Zhu, J. Fabrication of single-crystalline silicon nanowires by scratching a silicon surface with catalytic metal particles. *Adv. Funct. Mater.* **2006**, *16*, 387–394. [[CrossRef](#)]
57. Huang, Z.; Geyer, N.; Werner, P.; de Boor, J.; Gösele, U. Metal-assisted chemical etching of silicon: A review. *Adv. Mater.* **2011**, *23*, 285–308. [[CrossRef](#)] [[PubMed](#)]
58. Bryche, J.-F.; Bélier, B.; Bartenlian, B.; Barbillon, G. Low-cost SERS substrates composed of hybrid nanoskittles for a highly sensitive sensing of chemical molecules. *Sens. Actuator B* **2017**, *239*, 795–799. [[CrossRef](#)]
59. Magno, G.; Bélier, B.; Barbillon, G. Gold thickness impact on the enhancement of SERS detection in low-cost Au/Si nanosensors. *J. Mater. Sci.* **2017**, *52*, 13650–13656. [[CrossRef](#)]
60. Magno, G.; Bélier, B.; Barbillon, G. Al/Si nanopillars as very sensitive SERS substrates. *Materials* **2018**, *11*, 1534. [[CrossRef](#)]
61. Kara, S.A.; Keffous, A.; Giovannozzi, A.M.; Rossi, A.M.; Cara, E.; D’Ortenzi, L.; Sparnacci, K.; Boarino, L.; Gabouze, N.; Soukane, S. Fabrication of flexible silicon nanowires by self-assembled metal assisted chemical etching for surface enhanced Raman spectroscopy. *RSC Adv.* **2016**, *6*, 93649–93659. [[CrossRef](#)]
62. Cara, E.; Mandrile, L.; Lupi, F.F.; Giovannozzi, A.M.; Dialameh, M.; Portesi, C.; Sparnacci, K.; De Leo, N.; Rossi, A.M.; Boarino, L. Influence of the long-range ordering of gold-coated Si nanowires on SERS. *Sci. Rep.* **2018**, *8*, 11305. [[CrossRef](#)] [[PubMed](#)]
63. Lin, D.; Wu, Z.; Li, S.; Zhao, W.; Ma, C.; Wang, J.; Jiang, Z.; Zhong, Z.; Zheng, Y.; Yang, X. Large-area Au-nanoparticle-functionalized Si nanorod arrays for spatially uniform surface-enhanced Raman spectroscopy. *ACS Nano* **2017**, *11*, 1478–1487. [[CrossRef](#)] [[PubMed](#)]
64. Liang, Z.; Fan, D. Visible light-gated reconfigurable rotary actuation of electric nanomotors. *Sci. Adv.* **2018**, *4*, eaau0981. [[CrossRef](#)] [[PubMed](#)]
65. Peng, K.Q.; Lu, A.J.; Wong, N.B.; Zhang, R.Q.; Lee, S.T. Motility of metal nanoparticles in silicon and induced anisotropic silicon etching. *Adv. Funct. Mater.* **2008**, *18*, 3026–3035. [[CrossRef](#)]
66. Huang, J.-A.; Zhao, Y.-Q.; Zhang, X.-J.; He, L.-F.; Wong, T.-L.; Chui, Y.-S.; Zhang W.-J.; Lee, S.-T. Ordered Ag/Si nanowires array: Wide-range surface-enhanced Raman spectroscopy for reproducible biomolecule detection. *Nano Lett.* **2013**, *13*, 5039–5045. [[CrossRef](#)] [[PubMed](#)]

67. Lagarkov, A.; Boginkaya, I.; Bykov, I.; Budashov, I.; Ivanov, A.; Kurochkin, I.; Ryzhikov, I.; Rodionov, I.; Sedova, M.; Zverev, A.; et al. Light localization and SERS in tip-shaped silicon metasurface. *Opt. Express* **2017**, *25*, 17021–17038. [[CrossRef](#)]
68. Sarychev, A.K.; Ivanov, A.; Lagarkov, A.; Barbillon, G. Light concentration by metal-dielectric micro-resonators for SERS sensing. *Materials* **2019**, *12*, 103. [[CrossRef](#)] [[PubMed](#)]
69. Powell, J.A.; Venkatakrishnan, K.; Tan, B. Hybridized enhancement of the SERS detection of chemical and bio-marker molecules through Au nanosphere ornamentation of hybrid amorphous/crystalline Si nanoweb nanostructure biochip devices. *J. Mater. Chem. B* **2016**, *4*, 5713–5728. [[CrossRef](#)]
70. Chan, S.; Kwon, S.; Koo, T.W.; Lee, L.P.; Berlin, A.A. Surface-enhanced Raman scattering of small molecules from silver-coated silicon nanopores. *Adv. Mater.* **2003**, *15*, 1595–1598. [[CrossRef](#)]
71. Wu, Y.K.; Liu, K.; Li, X.F.; Pan, S. Integrate silver colloids with silicon nanowire arrays for surface-enhanced Raman scattering. *Nanotechnology* **2011**, *22*, 215701. [[CrossRef](#)] [[PubMed](#)]
72. Lu, R.; Sha, J.; Xia, W.W.; Fang, Y.J.; Gu, L.; Wang, Y.W. A 3D-SERS substrate with high stability: Silicon nanowire arrays decorated by silver nanoparticles. *CrystEngComm* **2013**, *15*, 6207–6212. [[CrossRef](#)]
73. Wang, S.-Y.; Jiang, X.-X.; Xu, T.-T.; Wei, X.-P.; Lee, S.-T.; He, Y. Reactive ion etching-assisted surface-enhanced Raman scattering measurements on the single nanoparticle level. *Appl. Phys. Lett.* **2014**, *104*, 243104. [[CrossRef](#)]
74. Ding, S.-Y.; You, E.-M.; Tian, Z.-Q.; Moskovits, M. Electromagnetic theories of surface-enhanced Raman spectroscopy. *Chem. Soc. Rev.* **2017**, *46*, 4042–4076. [[CrossRef](#)] [[PubMed](#)]
75. Li, J.-F.; Zhang, Y.-J.; Ding, S.-Y.; Panneerselvam, R.; Tian, Z.-Q. Core-shell nanoparticle-enhanced Raman spectroscopy. *Chem. Rev.* **2017**, *117*, 5002–5069. [[CrossRef](#)]
76. Ding, S.-Y.; Yi, J.; Li, J.-F.; Ren, B.; Wu, D.-Y.; Panneerselvam, R.; Tian, Z.-Q. Nanostructure-based plasmon-enhanced Raman spectroscopy for surface analysis of materials. *Nat. Rev. Mater.* **2016**, *1*, 16021. [[CrossRef](#)]
77. Cao, Y.C.; Jin, R.; Mirkin, C.A. Nanoparticles with Raman spectroscopic fingerprints for DNA and RNA detection. *Science* **2002**, *297*, 1536–1540. [[CrossRef](#)]
78. Erdélyi, R.; Nagata, T.; Rogers, D.J.; Teherani, F.H.; Horváth, Z.E.; Lábadi, Z.; Baji, Z.; Wakayama, Y.; Volk, J. Investigations into the impact of the template layer on ZnO nanowire arrays made using low temperature wet chemical growth. *Cryst. Growth Des.* **2011**, *11*, 2515–2519. [[CrossRef](#)]
79. Özgür, Ü.; Alivov, Y.I.; Liu, C.; Teke, A.; Reshchikov, M.A.; Doğan, S.; Avrutin, V.; Cho, S.-J.; Morkoç, H. A comprehensive review of ZnO materials and devices. *J. Appl. Phys.* **2005**, *98*, 041301. [[CrossRef](#)]
80. Janotti, A.; Van de Walle, C.G. Fundamentals of zinc oxide as a semiconductor. *Rep. Prog. Phys.* **2009**, *72*, 126501. [[CrossRef](#)]
81. Cheng, C.; Yan, B.; Wong, S.M.; Li, X.; Zhou, W.; Yu, T.; Shen, Z.; Yu, H.; Fan, H.J. Fabrication and SERS Performance of Silver-Nanoparticle-Decorated Si/ZnO Nanotrees in Ordered Arrays. *ACS Appl. Mater. Interfaces* **2010**, *7*, 1824–1828. [[CrossRef](#)] [[PubMed](#)]
82. Lee, Y.; Lee, J.; Lee, T.K.; Park, J.; Ha, M.; Kwak, S.K.; Ko, H. Particle-on-film gap plasmons on antireflective ZnO nanocone arrays for molecular-level surface-enhanced Raman scattering sensors. *ACS Appl. Mater. Interfaces* **2015**, *7*, 26421–26429. [[CrossRef](#)] [[PubMed](#)]
83. Fang, Y.; Wang, Y.; Wan, Y.; Wang, Z.; Sha, J. Detailed study on photoluminescence property and growth mechanism of ZnO nanowire arrays grown by thermal evaporation. *J. Phys. Chem. C* **2010**, *114*, 12469–12476. [[CrossRef](#)]
84. Zhu, G.; Zhou, Y.; Wang, S.; Yang, R.; Ding, Y.; Wang, X.; Bando, Y.; Wang, Z.L. Synthesis of vertically aligned ultra-long ZnO nanowires on heterogeneous substrates with catalyst at the root. *Nanotechnology* **2012**, *23*, 055604. [[CrossRef](#)]
85. Chen, L.; Luo, L.; Chen, Z.; Zhang, M.; Antonio Zapien, J.; Lee, C.S.; Lee, S.T. ZnO/Au composite nanoarrays as substrates for surface-enhanced Raman scattering detection. *J. Phys. Chem. C* **2010**, *114*, 93–100. [[CrossRef](#)]
86. Shan, Y.; Yang, Y.; Cao, Y.; Fu, C.; Huang, Z. Synthesis of wheatear-like ZnO nanoarrays decorated with Ag nanoparticles and its improved SERS performance through hydrogenation. *Nanotechnology* **2016**, *27*, 145502. [[CrossRef](#)]
87. Xu, J.-Q.; Duo, H.-H.; Zhang, Y.-G.; Zhang, X.-W.; Fang, W.; Liu, Y.-L.; Shen, A.-G.; Hu, J.-M.; Huang, W.-H. Photochemical synthesis of shape-controlled nanostructured gold on zinc oxide nanorods as photocatalytically renewable sensors. *Anal. Chem.* **2016**, *88*, 3789–3795. [[CrossRef](#)]

88. He, X.; Yue, C.; Zang, Y.; Yin, J.; Sun, S.; Li, J.; Kang, J. Multi-hotspot configuration on urchin-like Ag nanoparticle/ZnO hollow nanosphere arrays for highly sensitive SERS. *J. Mater. Chem. A* **2013**, *1*, 15010–15015.
89. Park, S.G.; Jeon, T.Y.; Jeon, H.C.; Kwon, J.D.; Mun, C.; Lee, M.; Cho, B.; Kim, C.S.; Song, M.; Kim, D.H. Fabrication of Au-decorated 3D ZnO nanostructures as recyclable SERS substrates. *IEEE Sens. J.* **2016**, *16*, 3382–3386. [[CrossRef](#)]
90. Song, W.; Ji, W.; Vantasin, S.; Tanabe, I.; Zhao, B.; Ozaki, Y. Fabrication of a highly sensitive surface-enhanced Raman scattering substrate for monitoring the catalytic degradation of organic pollutants. *J. Mater. Chem. A* **2015**, *3*, 13556–13562. [[CrossRef](#)]
91. Jayram, N.D.; Sonia, S.; Poongodi, S.; Suresh Kumar, P.; Masuda, Y.; Mangalaraj, D.; Ponpandian, N.; Viswanathan, C. Superhydrophobic Ag decorated ZnO nanostructured thin film as effective surface enhanced Raman scattering substrates. *Appl. Surf. Sci.* **2015**, *355*, 969–977. [[CrossRef](#)]
92. Xie, Y.; Yang, S.; Mao, Z.; Li, P.; Zhao, C.; Cohick, Z.; Huang, P.-H.; Huang, T.J. In situ Fabrication of 3D Ag@ZnO nanostructures for microfluidic surface-enhanced Raman scattering systems. *ACS Nano* **2014**, *8*, 12175–12184. [[CrossRef](#)] [[PubMed](#)]
93. Marci, G.; Augugliaro, V.; López-Muñoz, M.J.; Martín, C.; Palmisano, L.; Rives, V.; Schiavello, M.; Tilley, R.J.D.; Venezia, A.M. Preparation characterization and photocatalytic activity of polycrystalline ZnO/TiO₂ systems. 2. Surface, bulk characterization, and 4-Nitrophenol photodegradation in Liquid–Solid regime. *J. Phys. Chem. B* **2001**, *105*, 1033–1040. [[CrossRef](#)]
94. Zhou, Q.; Wen, J.Z.; Zhao, P.; Anderson, W.A. Synthesis of vertically-aligned zinc oxide nanowires and their application as a photocatalyst. *Nanomaterials* **2017**, *7*, 9. [[CrossRef](#)]



© 2019 by the authors. Licensee MDPI, Basel, Switzerland. This article is an open access article distributed under the terms and conditions of the Creative Commons Attribution (CC BY) license (<http://creativecommons.org/licenses/by/4.0/>).